

Metal-Insulator Transition in VO₂: A DFT + DMFT Perspective

W. H. Brito,^{1,2} M. C. O. Aguiar,¹ K. Haule,² and G. Kotliar²

¹*Departamento de Física, Universidade Federal de Minas Gerais, C. P. 702, 30123-970 Belo Horizonte, Minas Gerais, Brazil*

²*Department of Physics and Astronomy, Rutgers University, Piscataway, New Jersey 08854, USA*

(Received 9 September 2015; published 27 July 2016)

We present a theoretical investigation of the electronic structure of rutile (metallic) and M_1 and M_2 monoclinic (insulating) phases of VO₂ employing a fully self-consistent combination of density functional theory and embedded dynamical mean field theory calculations. We describe the electronic structure of the metallic and both insulating phases of VO₂, and propose a distinct mechanism for the gap opening. We show that Mott physics plays an essential role in all phases of VO₂: undimerized vanadium atoms undergo classical Mott transition through local moment formation (in the M_2 phase), while strong superexchange within V dimers adds significant dynamic intersite correlations, which remove the singularity of self-energy for dimerized V atoms. The resulting transition from rutile to dimerized M_1 phase is adiabatically connected to the Peierls-like transition, but is better characterized as the Mott transition in the presence of strong intersite exchange. As a consequence of Mott physics, the gap in the dimerized M_1 phase is temperature dependent. The sole increase of electronic temperature collapses the gap, reminiscent of recent experiments.

DOI: 10.1103/PhysRevLett.117.056402

VO₂ is of great practical importance as its metal-insulator transition (MIT) is very close to room temperature, and its ultrafast switching between metallic and insulating phases can be used for device applications [1]. VO₂ is also of fundamental interest, due to the complex interplay between electronic correlations and structural distortions, and as a result the physical mechanism responsible for the gap formation has remained under debate.

Structurally, VO₂ undergoes a transition from a high temperature rutile phase [2] (R) to low temperature monoclinic phases. In the latter, under ambient pressure, the vanadium atoms dimerize and tilt with respect to the rutile c axis, giving rise to the M_1 phase [3]. Because of the dimerization, it is expected that the electronic states associated with the overlapping d orbitals along the rutile c axis (a_{1g} states) split into bonding-antibonding subbands. In addition, the antiferroelectric displacement leads to an upshift of the subbands associated with the remaining t_{2g} states (e_g^π). As a result, a gap would appear between the a_{1g} and e_g^π subbands, suggesting thus that VO₂ undergoes a Peierls-type transition [4]. However, density functional theory (DFT) calculations showed that these structural distortions alone cannot give rise to a gap in the M_1 phase [5,6]. In addition, a distinct monoclinic phase (M_2) appears when the system is under uniaxial stress or doped with Cr³⁺, Al³⁺, Fe³⁺, or Ga³⁺ [7,8]. In this phase half of the vanadium atoms pair along the rutile c axis, while the other half experience a zigzag-like distortion along the same axis. In particular, the existence of localized electrons in the zigzag chains also suggests that electronic correlations indeed play a role in the gap formation of VO₂.

The cluster-dynamical mean field theory (DMFT) has successfully described several aspects of the physics of VO₂, but some discrepancies between different implementations remain. Biermann *et al.* [9] showed that the M_1 phase is insulating, with the gap of 0.6 eV in agreement with experimental findings [10]. Furthermore, the authors found that electronic intersite correlations, within the vanadium dimers, renormalize down the a_{1g} bonding-antibonding splitting in comparison with DFT calculations. In their proposed mechanism, the M_1 phase can be viewed as a renormalized Peierls insulator. In contrast, by means of *ab initio* linear scaling DFT + cluster-DMFT calculations, Weber *et al.* [11] observed that the gap formation of the M_1 phase is mainly due to an orbital-selective Mott instability concerning the a_{1g} electronic states in our notation. Looking at the occupancy of the 3d shell, they obtained at around two electrons per vanadium, resulting in four electrons per vanadium dimer, suggesting that the M_1 phase is *not* a renormalized Peierls insulator [9].

Important fundamental challenges remain: (i) the close proximity of the M_1 , M_2 , and R phase in the phase diagram [8,12] calls for a unified framework in which these phases can be simultaneously described; (ii) another fundamental question is whether the MIT transitions will take place if we fix the structure and change only the temperature.

It has not been possible to properly address these issues within an approach based on an effective model from which the oxygen degrees of freedom are eliminated, and which contains only V-3d electrons (Hubbard model). Indeed, earlier DMFT works on the Hubbard model [9,13,14] showed that for a given set of Hubbard U and J parameters, the gap in the M_1 insulating phase is too robust, persisting

to very high temperatures [9], while the mass renormalization in the R phase is too small compared to experiment [13,14]. Both of these effects result from placing this material too far from the Mott transition boundary. Consequently, the M_2 phase was not described before with this approach, as half of the V atoms would not undergo Mott-Hubbard transition.

In this Letter we solved these problems by describing VO_2 with a modern all electron embedded DMFT approach, where, in addition to correlated vanadium atoms, the itinerant states of oxygen are included in the Dyson self-consistent equation [15,16]. We present a comprehensive picture and describe all the phases of VO_2 with the same values of the (U, J) parameters, including the M_2 phase which has not been considered previously in DMFT treatments. Mott physics is central for the proper description of all the phases even though the Mott instability is arrested in the M_1 phase.

Our theory leads to a different physical picture for the gap opening in monoclinic phases of VO_2 , and most importantly the possibility of the *collapse* of the M_1 insulating state by temperature. Our results indicate the presence of significant intersite correlations within the vanadium dimers, which in turn lower the a_{1g} subband in relation to the e_g^π . In particular, we notice that nonlocal dynamic correlations *enhance* the a_{1g} bonding-antibonding splitting, in contrast to what was reported by Biermann *et al.* [9]. The electrons in all phases of VO_2 are in the near vicinity of the Mott transition, but the true pole in the self-energy, signaling the local moment formation, occurs only in the paramagnetic M_2 phase on undimerized V atoms and its a_{1g} orbital. In the M_1 phase and in the antiferro-ordered M_2 phase, the singularity of the self-energy is arrested as the ordered states are adiabatically connected to Peierls and Slater insulators, respectively. The adiabatic connection between the weakly and the corresponding strongly interacting states, makes the Mott mechanism hard to distinguish from alternative scenarios, nevertheless, collapsing a large insulating gap with raising electronic temperature is possible only in the Mott state in the presence of strong superexchange, as was found, for example, in the cluster-DMFT study of the 2D Hubbard model [40]. Hence, according to our results the M_1 phase is best characterized as the Mott phase in the presence of strong intersite superexchange within the V dimers, while the undimerized V atoms in the M_2 phase undergo canonical Mott transition associated with local moment formation in the presence of weak superexchange.

Rutile and M_1 phase.—We first address the R phase at temperature of 390 K. In Fig. 1(a) we show the calculated total, t_{2g} and e_g^σ projected density of states (DOS).

The R phase is metallic with strongly renormalized t_{2g} orbitals compared to corresponding DFT results (not shown). A weak lower Hubbard band (LHB) is observed at around -1.09 eV, and a broad upper Hubbard band

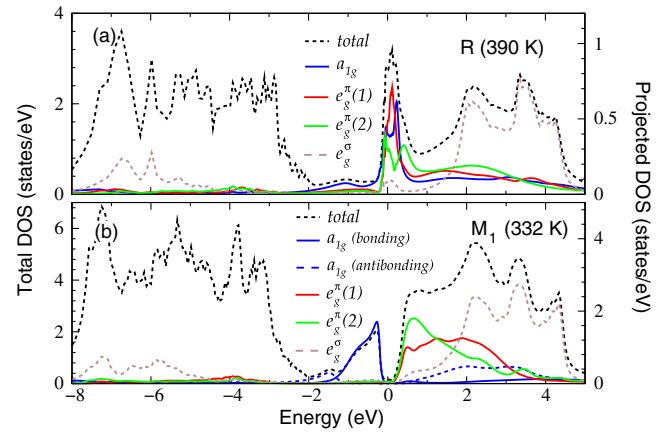


FIG. 1. DFT + DMFT-based total (black dashed line) and projected DOS of (a) R and (b) M_1 phase of VO_2 . The projections to a_{1g} , $e_g^\pi(1)$, $e_g^\pi(2)$, and e_g^σ states are shown in blue, red, green, and brown lines, respectively. For the M_1 phase, the solid (dashed) blue line corresponds to the projection on the bonding (antibonding) a_{1g} molecular state.

(UHB) at around 2.54 eV. The former is in good agreement with experimental photoemission measurements [10], and previous theoretical findings [9]. The LHB and UHB are mainly of a_{1g} and e_g^π character, respectively.

We next present the electronic structure of the M_1 phase. Within the V dimer, treated as a cluster in DMFT, it is useful to adopt the symmetric and antisymmetric combination of orbitals. The associated self-energies are denoted as the bonding $\Sigma_{b,\alpha}$ and antibonding $\Sigma_{ab,\alpha}$ components, where $\alpha = \{a_{1g}, e_g^\pi(1), e_g^\pi(2)\}$ [16]. In Fig. 1(b) the total, t_{2g} , and e_g^σ projected DOS are shown. At first, we notice the opening of a gap of 0.55 eV, between the a_{1g} and e_g^π subband, which is in good agreement with experimental and previous theoretical findings [9–11]. As expected, upon dimerization and antiferroelectric distortion, the a_{1g} subband splits in bonding (solid blue) and antibonding (dashed blue) states, while the e_g^π subband upshifts in comparison with the R phase. The a_{1g} bonding orbital has a coherent peak at around -0.30 eV, while the antibonding orbital has two incoherent peaks reminiscent of the LHB and UHB located at -1.5 eV and 2.58 eV, respectively. The coherent peak and the satellite below it were also observed in previous theoretical [9,14] and experimental [10] works. However, in our case, the UHB does not represent a weak coherent peak associated with the antibonding state, as in Ref. [9]. The bonding-antibonding splitting [relative to the DFT and DFT + single-site DMFT calculations (not shown)] increases upon inclusion of intersite dynamic correlations within the dimer, in contrast to Ref. [9].

We also computed the optical conductivity of R , M_1 , and M_2 phases of VO_2 , which are presented in Fig. 2(a). We calculate the plasma frequency of the R phase, defined as $\omega_p^2 = 2/(\pi\epsilon_0) \int_0^\Lambda \sigma(\omega) d\omega$, with $\Lambda = 2$ eV and

$\Lambda = 0.1$ eV, the latter denoted by ω_p^{*2} . At 390 K we obtained for the ratio $\omega_p^2(\text{LDA})/\omega_p^2(\text{DMFT}) = 2.24$, and $\omega_p(\text{DMFT}) = 3.28$ eV, in good agreement with Ref. [41]. We notice a mild temperature dependence of this ratio, decreasing with decreasing temperature. This signals an increase of kinetic energy due to gain of coherence, characteristic of a Mott-Hubbard system. On the other hand, the ratio $\omega_p^{*2}(\text{LDA})/\omega_p^{*2}(\text{DMFT})$ is much larger: at 100 K it is 4.71, and increases as the Drude peak broadens (at 390 K it is 6.12). Finally, the DMFT mass enhancements, extracted from the slope of the self-energy, are $m^*/m_{\text{band}} = 3.5, 3, 2.5$ for a_{1g} , $e_g^\pi(1)$, and $e_g^\pi(2)$, respectively. In the conventional Hubbard model picture, the mass enhancement (m^*/m_{band}) and the ratios of plasma frequencies [$\omega_p^2(\text{LDA})/\omega_p^2(\text{DMFT})$] should be very similar, and both are used to measure the correlation strength in the literature [42]. In VO₂ these measures of correlations differ because the plasma frequency ω_p includes substantial contribution from the interband transitions, which strongly mix with less correlated oxygen and e_g states, resulting in apparently weaker correlations than given by $m_{t_{2g}}^*/m_{\text{band}}$, a physics beyond the Hubbard model. The low energy ratio of ω_p^{*2} has negligible interband contribution, and at zero temperature it should be equal to $m_{t_{2g}}^*/m_{\text{band}}$, but at finite temperature it gets large due to broadening and the loss of strength of the Drude peak.

Effects of nonlocal dynamic correlations.—Having described the electronic structure of both R and M_1 phases of VO₂, we next investigate how nonlocal dynamic correlations contribute to the opening of a gap between a_{1g} and e_g^π subbands in the M_1 phase. Figure 2(c) shows the

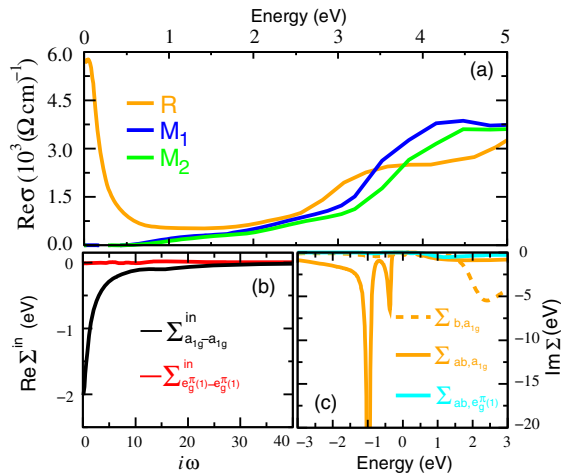


FIG. 2. (a) Real part of the optical conductivity of R , M_1 , and M_2 phases of VO₂. (b) Real part of intersite self-energies, on an imaginary frequency axis, of a_{1g} - a_{1g} (black) and $e_g^\pi(1)$ - $e_g^\pi(1)$ (red) states of M_1 phase. (c) Imaginary part, on real frequency axis, of bonding (dashed lines) and antibonding (solid lines) self-energies associated with the a_{1g} (orange) and $e_g^\pi(1)$ (cyan) dimer electronic states.

bonding and antibonding components of the imaginary part of the self-energy associated with the a_{1g} and $e_g^\pi(1)$ dimer electronic states.

We notice that once the Peierls instability occurs in our calculation, the Mott instability is arrested; hence, there is no pole in the imaginary part of the self-energy associated with the a_{1g} or e_g^π states. This excludes an orbital-selective Mott-Hubbard mechanism as the source of the gap of the M_1 phase, as proposed in Ref. [11]. Our results bear strong resemblance to the Mott transition of the Hubbard model in cluster-DMFT [43], where the local singlet state of the cluster dominates the low energy properties of the model. The energy gain to form the strong bonding state on the cluster is here not just due to increased hopping between the two V atoms, but it is primarily due to the gain of the exchange energy, which is stronger than kinetic energy, as the latter is strongly reduced due to proximity to the Mott transition. The precise calculation of this exchange energy is beyond this work since it requires the computation of the momentum dependent spin susceptibility which in turn depends on the two particle vertex function.

Next we define the local and intersite self-energies, which are related to the self-energies in the dimer basis as $\Sigma^{\text{local}} = \frac{1}{2}(\Sigma_b + \Sigma_{ab})$ and $\Sigma^{\text{in(ter)}} = \frac{1}{2}(\Sigma_b - \Sigma_{ab})$ [16]. In Fig. 2(b) we also show the real part of the intersite components of self-energies associated with the same electronic states as those in Fig. 2(c). We observe that the component of $e_g^\pi(1)$ is negligible, but, notably, one can see that $\text{Re}\Sigma_{a_{1g}-a_{1g}}^{\text{in}}$ depends strongly on the frequency in the low-energy part. This indicates the presence of strong intersite electronic correlations within the vanadium dimers, which in turn lower the a_{1g} bonding state. As a result, the bonding-antibonding splitting *increases* and a gap between the a_{1g} and e_g^π appears (for more details about the bonding-antibonding splitting see the Supplemental Material [16]). Thus, one can consider that nonlocal correlations give rise to an effective a_{1g} - a_{1g} frequency dependent hopping $t_{a_{1g}-a_{1g}} + \text{Re}\Sigma_{a_{1g}-a_{1g}}^{\text{in}}(i\omega)$, which properly takes into account the a_{1g} bonding-antibonding splitting. A similar observation was previously proposed for the low-temperature phase of Ti₂O₃ [44], but required a strong intersite Coulomb interaction for opening the gap.

Metallization due to hot carriers.—More recently, numerous experimental studies have reported the existence of monocliniclike metallic phases of VO₂ [45–49]. This transition was also induced by the application of femto-second laser pulses on VO₂ films. As pointed out by Wegkamp *et al.* [49], the photoexcitation gives rise to hot carriers, which have an associated temperature much higher than the lattice temperature. Motivated by this fact, we performed calculations considering a much higher temperature, i.e., $T = 900$ K, for electrons in the M_1 phase.

In Figs. 3(a) and 3(b) we show the calculated spectral function and the projected DOS of M_1 at 332 and 900 K,

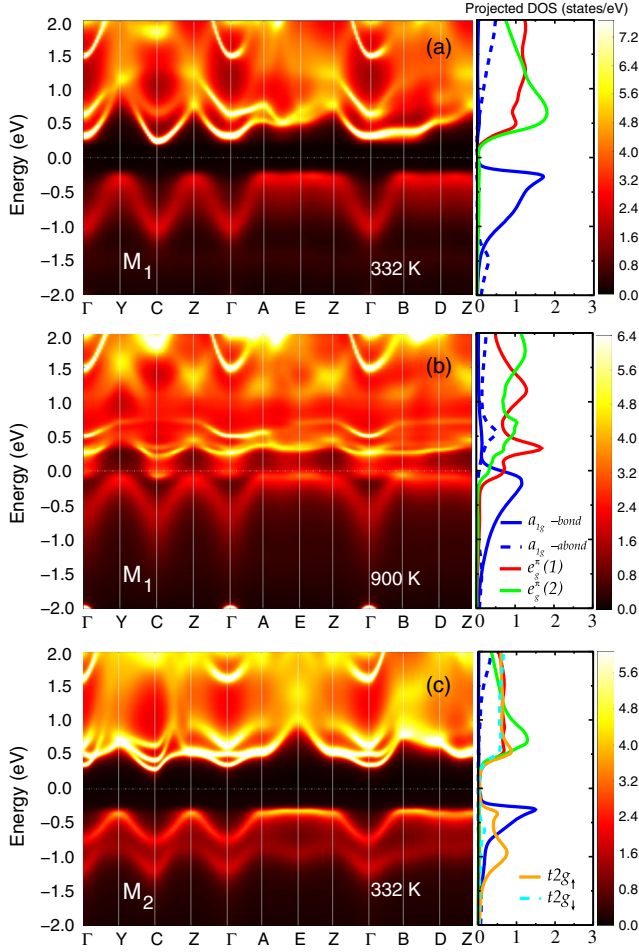


FIG. 3. Spectral function and projected DOS of M_1 phase at 332 K (a) and 900 K (b). In (c) the spectral function of M_2 phase at 332 K is shown.

respectively. From the spectral function at 900 K, one can see the closing of the gap. In particular, we observe that a_{1g} and $e_g^\pi(1)$ subbands shift towards the Fermi level, the latter shifting more than the a_{1g} subband. To understand why the gap vanishes at 900 K, we examine the temperature dependence of the self-energies. In Fig. 4(a) we present the real part of intersite $\Sigma_{a_{1g}-a_{1g}}^{\text{in}}$ for these two temperatures. In addition, in the inset we show the antibonding component of $\text{Re}\Sigma_{ab,a_{1g}}$ and the bonding component of $\text{Re}\Sigma_{b,e_g^\pi(1)}$, on the real frequency axis. Here, we observe that $\text{Re}\Sigma_{a_{1g}-a_{1g}}^{\text{in}}$, in the low-energy part, and $\text{Re}\Sigma_{ab,a_{1g}}$ are strongly suppressed with increasing temperature. Therefore at 900 K the renormalization of the a_{1g} subband decreases significantly in comparison to that at 332 K. Thus, this subband is shifted towards the Fermi level. In relation to the $e_g^\pi(1)$ subband, we note an enhancement of the $\text{Re}\Sigma_{b,e_g^\pi(1)}$ from -0.46 eV to 0.77 eV, leading to a downshift of this subband.

M_2 phase.—Our cluster-DMFT simulation of the M_2 phase, using the same values of U and J employed for the

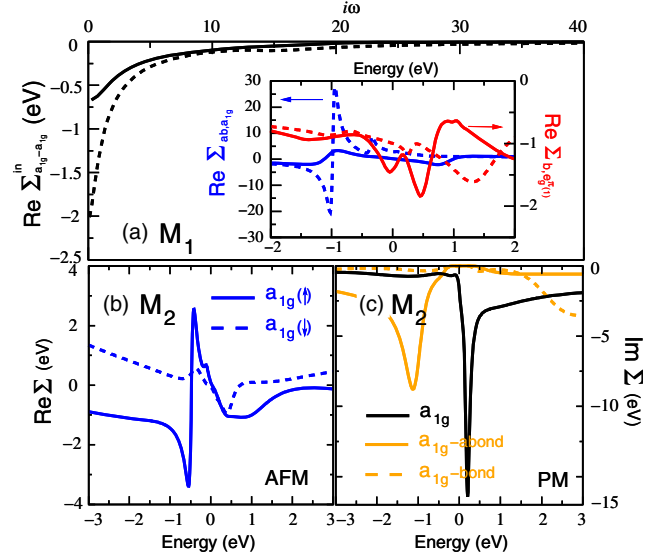


FIG. 4. (a) $\text{Re}\Sigma_{a_{1g}-a_{1g}}^{\text{in}}(i\omega)$ at 332 K (dashed lines) and 900 K (solid lines) of M_1 phase. Inset: $\text{Re}\Sigma_{ab,a_{1g}}(\omega)$ (blue) and $\text{Re}\Sigma_{b,e_g^\pi(1)}(\omega)$ (red) at 332 K (dashed lines) and 900 K (solid lines). (b) $\text{Re}\Sigma_{a_{1g}}(\omega)$ of undimerized V atoms in the antiferromagnetic phase of M_2 phase. (c) $\text{Im}\Sigma(\omega)$ of bonding and antibonding a_{1g} self-energies of V dimers (orange lines) and a_{1g} states of undimerized V atoms (black lines).

other phases, is presented in Fig. 3(c). The size of the insulating gap is ≈ 0.58 eV. In addition, we show in Fig. 2(a) the calculated optical conductivity of M_2 phase. Interestingly, we observe that both monoclinic phases are very similar, providing further support for the Mott point of view.

For this simulation we allowed antiferromagnetic ordering of undimerized vanadium atoms, but we find a similar gap also in the paramagnetic simulation of this phase. In both simulations, we find that the a_{1g} orbital on the dimerized V atoms is renormalized due to intersite correlations, in a similar way as in the M_1 phase. However, the splitting mechanism of the a_{1g} orbital on undimerized V atoms depends on the magnetic ordering. In particular, in the antiferromagnetic phase the a_{1g} orbital is renormalized by the spin-dependent real part of the local a_{1g} self-energy, which depends strongly on frequency in the low-energy part as shown in Fig. 4(b). In contrast, in the paramagnetic phase the a_{1g} self-energy has a pole in the imaginary part as can be seen in Fig. 4(c). This indicates that in the paramagnetic phase, the a_{1g} orbital of the undimerized V atoms splits due to the canonical Mott instability, proving that the M_2 phase should be characterized as a Mott insulator. In addition, this Mott instability also leads to an orbital polarization in favor of the a_{1g} orbital of undimerized V atoms by about $0.34/V$ atom with respect to the same orbital in R phase. It is noteworthy that the e_g^π orbital occupation decreases almost by the same amount ($-0.28/V$ atom). Finally, we mention that this orbital polarization leads to

the stabilization of the a_{1g} electronic states and therefore cooperates for the stabilization of the insulating state in the M_2 phase.

Conclusions.—Our work highlights the importance of simultaneously describing all phases of a strongly correlated material. The importance of Mott physics in all the phases of VO_2 was stressed early on in the pioneering work of Pouget and Rice [50]. This physics now emerges from a quantitative first principles method, and its implications for many physical quantities has been elucidated.

We acknowledge support from the Brazilian agencies CNPq, FAPEMIG, and CAPES. W. H. B. and M. C. O. A. acknowledge A. M. de Paula and V. B. Nascimento for useful discussions. K. H. and G. K. were supported by NSF DMR-1405303 and NSF DMR-1308141, respectively.

-
- [1] Z. Yang, C. Ko, and S. Ramanathan, *Annu. Rev. Mater. Res.* **41**, 337 (2011).
- [2] D. B. McWhan, M. Marezio, J. P. Remeika, and P. D. Dernier, *Phys. Rev. B* **10**, 490 (1974).
- [3] J. M. Long and P. Kierkegaard, *Acta Chem. Scand.* **24**, 420 (1970).
- [4] J. B. Goodenough, *Phys. Rev.* **117**, 1442 (1960).
- [5] R. M. Wentzcovitch, W. W. Schulz, and P. B. Allen, *Phys. Rev. Lett.* **72**, 3389 (1994).
- [6] V. Eyert, *Ann. Phys. (Berlin)* **11**, 650 (2002).
- [7] J. P. Pouget, H. Launois, J. P. D’Haenens, P. Merenda, and T. M. Rice, *Phys. Rev. Lett.* **35**, 873 (1975).
- [8] E. Strelcov, A. Tselev, I. Ivanov, J. D. Budai, J. Zhang, J. Z. Tischler, I. Kravchenko, S. V. Kalinin, and A. Kolmakov, *Nano Lett.* **12**, 6198 (2012).
- [9] S. Biermann, A. Poteryaev, A. I. Lichtenstein, and A. Georges, *Phys. Rev. Lett.* **94**, 026404 (2005).
- [10] T. C. Koethe, Z. Hu, M. W. Haverkort, C. Schüßler-Langeheine, F. Venturini, N. B. Brookes, O. Tjernberg, W. Reichelt, H. H. Hsieh, H.-J. Lin, C. T. Chen, and L. H. Tjeng, *Phys. Rev. Lett.* **97**, 116402 (2006).
- [11] C. Weber, D. D. O’Regan, N. D. M. Hine, M. C. Payne, G. Kotliar, and P. B. Littlewood, *Phys. Rev. Lett.* **108**, 256402 (2012).
- [12] J. H. Park, J. M. Coy, T. S. Kasirga, C. Huang, Z. Fei, S. Hunter, and D. H. Cobden, *Nature (London)* **500**, 431 (2013).
- [13] J. M. Tomczak, F. Aryasetiawan, and S. Biermann, *Phys. Rev. B* **78**, 115103 (2008).
- [14] B. Lazarovits, K. Kim, K. Haule, and G. Kotliar, *Phys. Rev. B* **81**, 115117 (2010).
- [15] K. Haule, C.-H. Yee, and K. Kim, *Phys. Rev. B* **81**, 195107 (2010).
- [16] See Supplemental Material at <http://link.aps.org/supplemental/10.1103/PhysRevLett.117.056402> for more details about the method, which includes Refs. [17–39].
- [17] X. Deng, A. Sternbach, K. Haule, D. N. Basov, and G. Kotliar, *Phys. Rev. Lett.* **113**, 246404 (2014).
- [18] K. Haule, T. Birol, and G. Kotliar, *Phys. Rev. B* **90**, 075136 (2014).
- [19] H. Zhang, K. Haule, and D. Vanderbilt, *Phys. Rev. Lett.* **111**, 246402 (2013).
- [20] K. Ohta, R. E. Cohen, K. Hirose, K. Haule, K. Shimizu, and Y. Ohishi, *Phys. Rev. Lett.* **108**, 026403 (2012).
- [21] M. K. Stewart, C.-H. Yee, J. Liu, M. Kareev, R. K. Smith, B. C. Chapler, M. Varela, P. J. Ryan, K. Haule, J. Chakhalian, and D. N. Basov, *Phys. Rev. B* **83**, 075125 (2011).
- [22] Z. P. Yin, K. Haule, and G. Kotliar, *Nat. Phys.* **10**, 845 (2014).
- [23] S. Mandal, R. E. Cohen, and K. Haule, *Phys. Rev. B* **90**, 060501 (2014).
- [24] G. Lee, H. S. Ji, Y. Kim, C. Kim, K. Haule, G. Kotliar, B. Lee, S. Khim, K. H. Kim, K. S. Kim, K.-S. Kim, and J. H. Shim, *Phys. Rev. Lett.* **109**, 177001 (2012).
- [25] M. Janoschek, P. Das, B. Chakrabarti, D. L. Abernathy, M. D. Lumsden, J. M. Lawrence, J. D. Thompson, G. H. Lander, J. N. Mitchell, S. Richmond, M. Ramos, F. Trouw, J.-X. Zhu, K. Haule, G. Kotliar, and E. D. Bauer, *Sci. Adv.* **1**, e1500188 (2015).
- [26] J.-X. Zhu, R. C. Albers, K. Haule, G. Kotliar, and J. M. Wills, *Nat. Commun.* **4**, 2644 (2013).
- [27] X. Deng, K. Haule, and G. Kotliar, *Phys. Rev. Lett.* **111**, 176404 (2013).
- [28] B. Chakrabarti, M. E. Pezzoli, G. Sordi, K. Haule, and G. Kotliar, *Phys. Rev. B* **89**, 125113 (2014).
- [29] H. C. Choi, K. Haule, G. Kotliar, B. I. Min, and J. H. Shim, *Phys. Rev. B* **88**, 125111 (2013).
- [30] H. C. Choi, B. I. Min, J. H. Shim, K. Haule, and G. Kotliar, *Phys. Rev. Lett.* **108**, 016402 (2012).
- [31] D. Mazumdar, K. Haule, J. J. Yang, G. L. Pascut, B. S. Holinsworth, K. R. O’Neal, V. Kiryukhin, S.-W. Cheong, and J. L. Musfeldt, *Phys. Rev. B* **91**, 041105 (2015).
- [32] S. Mandal, R. E. Cohen, and K. Haule, *Phys. Rev. B* **89**, 220502 (2014).
- [33] I. Leonov, V. I. Anisimov, and D. Vollhardt, *Phys. Rev. B* **91**, 195115 (2015).
- [34] J. P. Perdew, K. Burke, and M. Ernzerhof, *Phys. Rev. Lett.* **77**, 3865 (1996).
- [35] P. Blaha, K. Schwarz, G. K. H. Madsen, D. Kvasnicka, and J. Luitz, *WIEN2K, An Augmented Plane Wave+Local Orbitals Program for Calculating Crystal Properties* (Karlheinz Schwarz, Techn. Universität Wien, Austria, 2001).
- [36] K. Haule, *Phys. Rev. B* **75**, 155113 (2007).
- [37] T. Maier, M. Jarrel, T. Pruschke, and M. H. Hettler, *Rev. Mod. Phys.* **77**, 1027 (2005).
- [38] G. Kotliar, S. Y. Savrasov, G. Palsson, and G. Biroli, *Phys. Rev. Lett.* **87**, 186401 (2001).
- [39] K. Haule and T. Birol, *Phys. Rev. Lett.* **115**, 256402 (2015).
- [40] H. Park, K. Haule, and G. Kotliar, *Phys. Rev. Lett.* **101**, 186403 (2008).
- [41] K. Okazaki, S. Sugai, Y. Muraoka, and Z. Hiroi, *Phys. Rev. B* **73**, 165116 (2006).
- [42] M. M. Qazilbash, K. S. Burch, D. Whisler, D. Shrekenhamer, B. G. Chae, H. T. Kim, and D. N. Basov, *Phys. Rev. B* **74**, 205118 (2006).
- [43] K. Haule and G. Kotliar, *Phys. Rev. B* **76**, 104509 (2007).
- [44] A. I. Poteryaev, A. I. Lichtenstein, and G. Kotliar, *Phys. Rev. Lett.* **93**, 086401 (2004).

- [45] H.-T. Kim, Y. W. Lee, B.-J. Kim, B.-G. Chae, S. J. Yun, K.-Y. Kang, K.-J. Han, K.-J. Yee, and Y.-S. Lim, *Phys. Rev. Lett.* **97**, 266401 (2006).
- [46] E. Arcangeletti, L. Baldassarre, D. Di Castro, S. Lupi, L. Malavasi, C. Marini, A. Perucchi, and P. Postorino, *Phys. Rev. Lett.* **98**, 196406 (2007).
- [47] Z. Tao, T.-R. T. Han, S. D. Mahanti, P. M. Duxbury, F. Yuan, and C.-Y. Ruan, K. Wang, and J. Wu, *Phys. Rev. Lett.* **109**, 166406 (2012).
- [48] J. Laverock, S. Kittiwatanakul, A. A. Zakharov, Y. R. Niu, B. Chen, S. A. Wolf, J. W. Lu, and K. E. Smith, *Phys. Rev. Lett.* **113**, 216402 (2014).
- [49] D. Wegkamp, M. Herzog, L. Xian, M. Gatti, P. Cudazzo, C. L. McGahan, R. E. Marvel, R. F. Haglund, Jr., A. Rubio, M. Wolf, and J. Stähler, *Phys. Rev. Lett.* **113**, 216401 (2014).
- [50] T. M. Rice, H. Launois, and J. P. Pouget, *Phys. Rev. Lett.* **73**, 3042 (1994).